Exp. Theo. NANOTECHNOLOGY 8 (2024) 51-66 https://doi.org/10.56053/8.3.51

Fabrication and structural characterisation of ZrC-W cermet by spark plasma sintering: Application in ballistical projection

Badis Bendjemil[1,*], *Maram Mechi*[2], *Khaoula Safi*[3], *Mounir Ferhi*[2], *Karima Horchani Naifer*[2]

[1]Laboratory of applied mechanic and novel nanomaterials, University of 08 May 1945 Guelma, avenue 19 May 1956, CS 401, 24000 Guelma, Algeria
[2]Physical Chemistry Laboratory for Mineral Materials and their Applications, National Center for Research in Materials Sciences CNRSM, Technopole Borj Cedria, Tunisia
[3]LMS Laboratory, University of 8 May 1945 Guelma, avenue 19 May 1956, CS 401, CS 24000 Guelma, Algeria
[*]) Email: Badis23@ymail.com

Received 17/7/2024, *Received in revised form* 13/9/2024, *Accepted* 17/9/2024, *Published* 15/10/2024

This paper describes the effect of addition of tungesten (W) when was introduced into ZrC composite forming ceramic metal-composite (MMC) and (FGMS) to improve the fracture toughness (K_{IC}) and hardeness (Hv) of the composite ceramic-metal. ZrC and ZrC with addition of 20 % of tungesten (ZrC-W) were prepared by vacuum sintering FAST-SPS-FCT technology at the temperatures in the range of 1700–1800 °C for 400 s under pressure of 50 Mpa. Microtructural properties were investigated by X-ray diffraction and energy-dispersive spectrometry in addition scanning electron miroscopy. The investigations shows that the phase separation of the as-sintered ZrC and ZrC-20 wt%W into two phases: ZrC (dark) and (C)W (bright) indicating that the as-sintered (ZrC)W was thoroughly decomposed in tree phases ZrC, W2C and WC. The effect of the W is already illustrated. X-ray diffraction and energy-dispersive spectrometry results indicate that bright grains are W, (W)C and dark ZrC solid solution. The relative density increases with the reinforcement by W into ZrC. Fully dense ZrC and ZrC-20 vol% W ceramic metal-composite with a relative density of more than 98.8 % were obtained. The Vickers hardennes (HV), fracture toughness (KIC) and Raman spectroscopy will be performed in the near future. In addition, ballistic performance (dynamic properties by projectil persing resistance) . A finite element simulation will used to optimise the vol% W addition to obtain better mechanical properties and ballistical performance. The Analyzer of the termo-mechanical evolution within the volume of ZrC and ZrC-W specimens subjected to FAST-SPS-FCT platform (thermo-mechanical modeling under ABAQUS). Also, the ballistic performance will be evaluated using the Rosenberg model and compared with the experimental results in order to better understand the dynamic shock behavior of ceramic metal-composite (ZrC and ZrC-W) by the projectile that to be applied for body armor.

Keywords: FAST-SPS-FCT technology; Ceramic Metal-Composite; FGMs; Mechanical properties; Composite armor; Body armor.

1. INTRODUCTION

In a current context of decreasing polluting emissions, decreasing operating costs and increasing vehicle autonomy, the reduction of structures has become a major challenge for the industry. In the field of defence, ballistic protection necessary to guarantee the physical integrity of the occupants involve a substantial addition of mass which is detrimental to the mobility and autonomy of the vehicles. Efforts are therefore focused on the development of more efficiente and lighter protection systems that are accompanied by general of an additional cost. The systems selected are called "double hardness", composed of surface masses of several shielding systems sufficient to stop a piercing ammunition compared to their relative cost [1] of a hard layer on the front face intended to deform the projectile and a more ductile layer to stop the fragments. Aluminum alloys, some of which are currently used in ballistic protection, stand out as one of the lightest metallic materials and have a good deformation capacity to absorb the kinetic energy of fragments (projectile and armor) by deformation. The choice of B_4C boron carbide ceramic because of its very high hardness (3rd hardest material after diamond and BN boron nitride [2]) and its low density (2.52 g/cm^3). To increase the mechanical properties of aluminium, several ways are considered: the composition of the alloy, its metallurgical state, the process used and the size of the resulting grains. Finally, it is also possible to include hard ceramic type particles.
The Al-Zn-Mg type composition because this alloy belongs to a family of structural hardening alloys [3]. As far as the process is concerned, the powder route was chosen because it makes it possible to obtain ultrafine grains and to integrate reinforcements without any problem of wettability [4]. Since B_4C is light and used in the field of ballistic protection [5], it is particles of this nature that will be introduced to produce composites with a metal matrix.

Optimization of the grinding time of an Al-Zn-Mg powder to obtain a nanostructured material. Then, the study of the microstructure modifications induced during the consolidation by FAST-SPS-FCT technology. The mechanical properties were also evaluated under quasi-static and dynamic conditions. The analytical models will make it possible to quantify the contributions to the reinforcement and the study of the interest of grinding during the development of the metallic material by way of powders. The ballistic impact resistance properties will be evaluated a priori using the Rosenberg model. In response to the advancements in the design of weapons, intensive efforts have been undertaken to develop the next generation of lightweight armor structures with a higher level of ballistic performance while maintaining maneuverability. Typical multiple-layered composite armor systems, consisting of a high-impedance front plate backed by a ductile metal, have been extensively studied in armor applications [1-4]. However, the reflected waves caused by the impedance mismatch of ceramics and metals can induce a large number of ceramic fractures, making layered armors only useable for single impact applications [5]. Therefore, due to their distinctive features, functionally graded materials (FGMs) have been increasingly used as an advanced engineering solution for armor technologies. FGMs, typically consisting of metal and ceramic components, are characterized by varying volume fractions of constituent materials gradually or continuously across entire dimensions. This allows material properties to be tailored to meet the desired armored assemblies through functionally graded design [6,7].

FGMs combine the prominent characteristic features of ceramic and metal in a single volume. The hard outer layer is efficient in blunting and eroding the projectile, whereas the tough inner layer stops the projectile via absorbing its kinetic energy upon impact [8]. In addition, the smooth transition between the adjacent components is promising to attenuate the stress reflection waves that delay the failure of individual components [9]. As such, FGMs provide effective protection against ballistic threats while preventing structural breakdown by maintaining structural integrity. As such, FGMs are considered potential candidates for armor material in severe environments requiring anti-multiple

projectile impacts and high ballistic performance. The impact response and ballistic behavior of ceramic/ metal FGMs have been investigated in part of the literature. Pettersson et al. [10] explored the ballistic response of TiB_2 reinforced FGMs fabricated by spark plasma sintering (SPS). The results revealed that the FGMs exhibited superior ballistic resistance to the monolithic TiB_2. McCauley et al. [11] performed an experimental study on the ballistic properties of TiB_2-TiB-Ti FGMs and found that the FGMs with four or six layers were comparable to the baseline monolithic TiB_2. Gupta et al. [12] analyzed the ballistic properties of TiB_2-Ti based FGMs with respect to ballistic efficiency and penetration depth subjected to small caliber armor-piercing bullets. In this experiment, the FGMs showed lower ballistic performance than monolithic TiB_2 composites. Balcı et al. [13] adopted the hot-pressing technique to produce three-layered B_4C/AA7075 FGMs and studied their ballistic performance. The ballistic test results, using 7.62 mm armor-piercing (AP) projectiles, demonstrated that the performance of FGMs was significantly lower than that of Al_2O_3/Al laminated composites and Al_2O_3/ 4340 steel. In another similar study reported by Ubeyli et al. [14], the 40-20 vol% and 20-10 vol% SiC/7075Al FGMs did not exhibit improved ballistic resistance under the impact of 7.62 mm AP projectiles. Chao et al. [15] manufactured threelayered B_4C/AA2024 FGMs using squeeze casting technology, and the ballistic behavior was examined using 7.62 mm armor-piercing incendiary (API). It was reported that the FGM displayed a 14% decrease in the areal density of penetration than the homogeneous composite. It is evident that most of the existing FGM armor systems fail to achieve the expected defensive performance. Based on the different gradient architectures, FGMs can be divided into discretely-layered and continuously-graded configurations, which possess discretely and continuously changing properties across layers, respectively [16]. The FGMs used in ballistic attacks already reported are mostly discretely layered structures with relatively sharp interfaces. Although sharp interfaces are somewhat weakened in the piecewise FGMs, the existence of macroscopic interfaces can yield unfavorably large interlaminar stresses and finally delamination between layers under extreme dynamic conditions due to abrupt changes in material properties across interfaces. For instance, the honeycomb sandwich structures with Al6061/B_4CFGM face plates prepared by Arslan et al. [17] underwent delamination at inter layer regions after 0.30 caliber fragment simulating projectile impact. Again, Aydin et al. [18,19] also observed severe interlayer damage in the SiC/6061Al FGMs under high-velocity impact. Furthermore, there often exist residual pores and cracks in the interlayer interfaces and gradient layers with high ceramic contents [13, 14, 18], which deteriorates the ballistic resistance capability of FGM targets. In contrast to discretely layered structures, continuous FGMs with smooth interfaces can minimize or eliminate stress concentrations and singularities at interface corners [20]. Berezovski et al. [21] numerically investigated stress wave propagation in FGMs through the composite wave propagation algorithm. It was revealed that in a continuously graded structure with smooth transition between the components, the amplitude of tensile stresses was significantly lower than that in a step-wise graded structure, and the continuous FGMs were the best choice for the suppression of tensile and compressive stresses. Hence, FGMs without abrupt interfaces are considered an ideal architecture for protective equipment, which can gain high levels of ballistic performance by prolonging the time for the strike face to erode the incoming projectile. However, the bulk FGMs with smooth interfaces have not been effectively realized in any armor materials to date, which remains an open challenge. Given the complex architecture of FGMs, an optimized functionally graded design is essential to achieve a high protective performance of materials [22, 23]. Several studies suggest that the gradient distribution has become a critical consideration in altering the impact behavior and determining the structural design for armored plate applications. For example, Bruck [9] developed a one-dimensional model to examine the effects of the gradient architecture of FGMs on the attenuation of stress waves, and discovered that the time delay to the reflected wave propagation was primarily dependent on the composition gradient. Li et al. [24] computationally examined the propagation of stress waves through layered and graded metal-ceramic FGMs. The authors mentioned that the wave propagation within FGMs involved a complex coupling of elastic and viscoplastic response, Kleponis et al. [25] used computational modeling to point out that the traveling path of a projectile, such as soft to hard

surface or hard to soft surface along the thickness, played an important role in the penetration depth. Wang et al. [26] simulated the ballistic performance of four kinds of AlN-Al FGMs and achieved the best gradient index. Wang et al. [27] numerically studied the ballistic properties of TiC-TiB2 75 %vol and AlCoCrFeNi FGMs, and found that the anti-penetration performance enhanced with increasing unevenness of the ceramic distribution. Aydin et al. [18] compared the ballistic performance of SiC-6061Al FGMs with different ceramic compositions using 9 mm parabellum projectiles. The results showed that the graded plates with linear composition exhibited the optimum ballistic impact resistance, and the composition variation through thickness dramatically affected the bulletproof performance of the overall system. Gunes et al. [28-30] studied the influence of compositional gradient exponent, layer number and impactor velocity on the elastic impact response of SiC-Al FGM plates under lowvelocity impact loading. They noted that the compositional gradient exponent and impactor velocity affected considerably the impact behavior, but the number of layers had a minor effect. However, we observed that most reported works concerning the structural design of FGMs focused on computational techniques or low-velocity impact analysis. The ballistic response and protective mechanism of ceramic/metal FGMs exposed to high-velocity impact conditions based on a combination of experimental and numerical are insufficiently studied, and the corresponding optimal structural design is still limited.

Tungsten (W), a refractory metal, has the highest melting point (3410 °C) among metals and has been recognized as an ultra-high temperature material due to its high strength, elastic modulus, and corrosion resistance, and low coefficient of thermal expansion [31, 32]. ZrC has a similar melting point (3540 °C) and thermal expansion coefficient to those of W [32, 33]. W and ZrC have been evaluated as suitable materials for fabricating ultra-high temperature ceramics (UHTCs) because they exhibit mutual solubility at high temperatures and are unreactive [34, 37, and 38]. UHTCs include the carbides, nitrides, and borides of transition metals with outstanding characteristics in high-temperature environments, such as high melting points, thermal conductivities, thermal stabilities, and chemical and oxidation resistances, and low densities [39], making them suitable for a wide range of high-temperature applications. UHTCs are characterized by their extraordinarily high melting points, often over 3000 °C, which make them highly resistant to thermal degradation and phase changes under extreme conditions. The unique combination of properties exhibited by UHTCs, including high hardness, excellent thermal stability, and chemical resistance, make them promising candidates for demanding environments where traditional materials cannot be applied. There are various sintering methods for fabricating W-ZrC composites, namely hot-pressing, spark plasma sintering using a powder mixture of W and ZrC as the starting materials, and sintering precursor powders through an in-situ synthetic reaction. Previous studies have reported the fabrication and characteristics of W-ZrC composites (or cermets) through in-situ reactions using different powder precursors [35, 36, 38], where WC, ZrO_2, and $ZrSiO_4$ precursors were used for the in-situ synthesis of W and ZrC. Distinct products (such as W, W_2C, and ZrC) were formed through phase decomposition owing to the decarburization of WC and synthesis reactions between WC and ZrO_2 at high temperatures (near 1400 °C). The reported high-temperature phase decomposition and phase synthesis reactions [40] were used to fabricate W-ZrC. Manufacturing of TiC-ZrC composite was intensevely studied by several researcher and reinfoced by nanoWC and carbone to prtforme theirs balistical perfermance [41]. The additive manufacturing of spherical powder W–1%ZrC for was successfully fabricated by spray granulation combined with radio frequency (RF) plasma spheroidization. 3 μm tungsten powders and the nanosized ZrC powder were spray granulated into a porous agglomerated powder and then spheroidized to form a dense spherical powder by RF plasma and the laser powder bed fusion process. Spherical W–ZrC powder with a narrow particle size distribution and a uniform distribution of Zr element was obtained [42-45]. In this paper is presented first preminary results from structural properties, phases, microstructural analysis and densification behavior of the ceramics ZrC and composite ZrC-20Vol% W produced by FAST-SPS-FCT are presented. The ballistic perfermance will investigated by comparaison using experimental results and

simulation with the Rosenberg model in order to better understand the dynamic shock behavior of the composites and FGMs manufacturated that demonstrating their potential applications in industries such as aerospace, defense, and nuclear energy, where high-temperature materials with superior performances are indispensable.

2. EXPERIMENTAL

2.1 Starting Material

ZrC (purity: 98%; Kojundo Chemical Laboratory, Sakado, Japan) and W (purity: 98.5 %; Kojundo Chemical Laboratory, Sakado, Japan) powders were used as starting materials. The ZrC powders were mixed with W composition of 20 vol.%) and then ball- milled for 20 ks in an agate bottle using zirconia balls with a small amount of ethanol. The mixed powders were oven-dried at 340 K for 80 ks and passed through a 200-mesh sieve forming composite A. the ZrC powder is noted Ceramic A. The specimens were mirror-polished using diamonds lurry (1 μm). The crystal phases and lattice parameters were examined by X-ray diffraction (XRD, θ–2θ, Cu-K_α, Brucker, Tokyo, Japan). Microstructures were observed by scanning electron microscopy (SEM, Hitachi, Tokyo, Japan). The HV and K_{IC} values will be measured at room temperature by a Vickers hardness tester (HM-221, Mitutoyo, Tokyo, Japan) at load 1.96 N. K_{IC} will be calculated from Eq. (1):

$$\mathbf{K_{IC}} = 0.016(E/H_v)^{1/2}(P/c^{3/2}) \quad (1)$$

where E is Young's modulus and c is the half lengths of the crack formed around the corners of indentation. Young's moduli of ZrC, ZrC-W and W are 440, 522, and 410 GPa, respectively, and Young's moduli of the composites were estimated by the rule of mixtures.

2.2 Synthesis of composite and nanocomposites by FAST-SPS-FCT technology

Consolidation of Powders via Spark Plasma Sintering The field assisted sintering Technics-Spark Plasma Sintering technology (FAST-SPS-FCT) technology is an effective technique for the compaction of powder materials. A main characteristic of this method is the direct heating of the pressing tool and/or the sample by pulsed direct electrical current with low voltage. This results in high heating rates and allows for short treatment times in order to obtain highly compacted sinter bodies. The material transport (e.g. by diffusion) occurring during the sintering process can also be used for performing chemical reactions. Especially the conditions during the FAST-SPS process allow the use of the method also as an alternative synthesis route for nano-composites, of which, some can be obtained only with difficulties by other techniques. The ball-milled powders were consolidated via FAST-SPS-FCT method under high vacuum conditions using graphite die and punch at an applied external pressure of 50 MPa. In order to prepare high density compacts with negligible porosity, temperature and compression pressure was programmed to rise simultaneously, until stabilized to the maximum temperature and compression pressure, followed by holding the system at the same sintering conditions for 1.6 ks. Circular compacts with diameter 20 mm and thickness 4 mm were prepared using FAST- SPS-FCT. The sintering conditions used in this study are provided in Table 1. The five sintering schedules are represented in the (Figure 1).

The resulting samples of ZrC and ZrC-20 vol% W were sintered or SPSed by FAST-SPS-FCT in graphite dies (inner diameter of 20 mm) coated with graphite sheet lubricant atomized with cBN at 1273 to 1473°K in vacuum. The Table 1 presented the sintering condition of the TiC- based nano-composites. The applied pressure 50 MPa was adjusted to the powder at room temperature and kept constant throughout the hot-pressing process. The pressure was applied at the beginning of the sintering process because high green density is favorable for better densification rate by reducing the pores prior to the densification during heating. The heating rate was about 10°C/min and the dwelling

time at terminal temperature was 60 min. The temperature was measured by an infrared pyrometer through a hole opened in the graphite die. Furthermore, for monitoring densification process, the shrinkage of the powder compact was measured by a displacement sensor during the sintering. The dimensions of the finally sintered samples were about 20 mm in diameter and 3 mm in thickness after calculation of their weight using the densities values. The mixtures were loosely compacted into a graphite die of 20 mm in diameter and sintered in the vacuum (1 Pa) at various temperatures using an FAST-SPS-FCT apparatus at the sinter Labs**:** Laboratoire Interdisciplinaire Carnot de Bourgogne (ICB), 9 AV Alain Savary, 21000 Dijon- France.

(a)

(b)

Figure 1 Sintered samples with die diameter of 20 mm: (**a**) Ceramic carbide A, (**b**) Composite Ceramic-Metal A or cermets.

A constant heating rate of 120°C/min was employed, while the applied pressure was 50 MPa. The on/off time ratio of the pulsed current was set to 10/2 in each run. The maximum current reached approximately 3000 A during sintering. recorded in order to analyze the synthesis and sintering. The sintered samples are presented in the Figure 1. Densities of the sintered samples was measured by the Archimedes' using the densimeter type Micromiritics Accupyc 1330. In Table 1 the FAST-SPS-FCT technology synthesis parameters were presented.

Table 1 FAST-SPS-FCT technology synthesis parameters.

SPSed Samples	T (°C)	Time of the cycle (mn)	Heating rate (C/min)	P (MPa)	Die (mm)
Ceramic ZrC	1700	8	10	50	20
MMC ZrC-W	1700	8	10	50	20

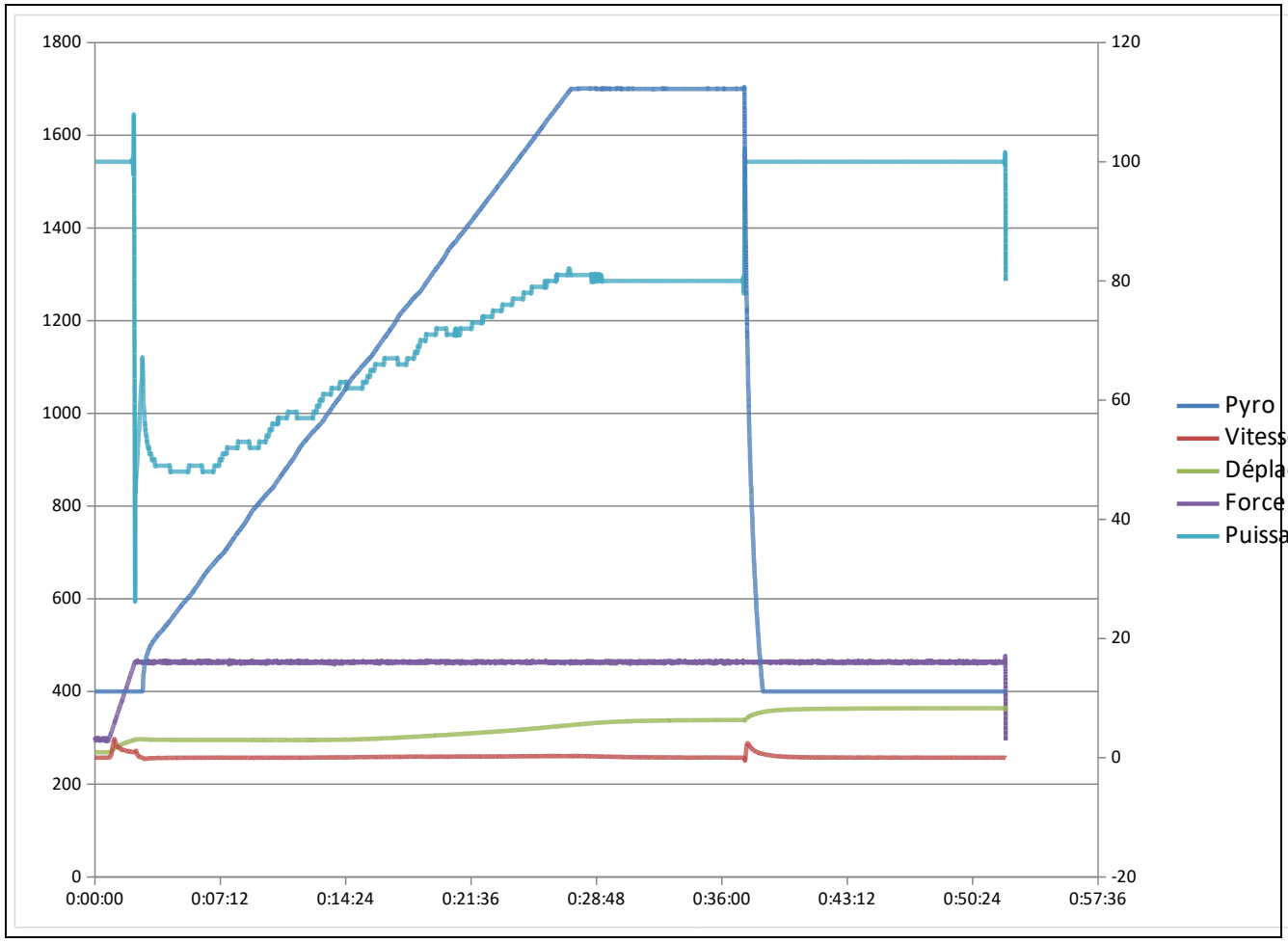

Figure 2 Variation of die displacement or shrinkage, temperature and applied pressure in dependence on the heating time during the FAST-SPS-FCT technology SPSed samples.

The composite ZrC-W and ceramic carbide ZrC (denoted as CompA–CeramA) were designed with different additions. The chemical compositions and the powder sizes of the nano-composites are listed in Table 2.

Table 2 Chemical compositions and powder sizes of the designed composite and ceramic carbie.

	CeramA (0.88 μm)	CompA (0.88 μm)
Carbide Ceramic ZrC	100 (vol.%)	
Composite Metallic Matrix Ceramic ZrC-W		80-20 (vol. %)

The microstructure o polished specimen was observed by optical microscopy and scanning electron microscopy (SEM) in back scattered electron mode, in conjunction with an energy-dispersive spectrometry (EDS). The element distribution in different phases was characterized by EDS. The phase identification of the nano-composites was carried out by an X-ray diffractometer. The measurement of relative density was conducted by Archimedes method, which was described in previous literature [46-49].

3. RESULTS AND DISCUSSION

3.1 Structural properties

3.1.1 Densification behavior

Densification of ZrC and ZrC-W composite was examined by the displacement of a graphite punch during sintering, i.e., from shrinkage curves. Figure 2 displays the effects of the nominal composition on shrinkage curves. at 400–1700 °C and the time dependence of isothermal displacements at 1700 °C up to 500 s. The displacement was more significant than that of the monolithic ZrC, as shown in Figure 2; the shrinkage of the monolithic ZrC started at 1100 °C and proceeded up to 1700 °C, whereas the monolithic ZrC started to shrink above 1400 °C. For the composites ZrC-20Vol% W, the displacement in ZrC-20 vol.% composite A began at approximately 1100 °C and the composite gradually shrunk as the sintering temperature increased from 1100 to 1700 °C, as shown in Figure 2.

3.1.2 Phase formation of solid solutions of ZrC-20vol.% W composite

The phase formation of solid solutions of ZrC ceramic carbide SPSed at 1700 °C is illustrated in the Figure 3a reflection peaks of the starting mixture powders, ZrC (JCPDS 35-0784) are included for comparison. Figure 3b depicts the effects of additions 20 vol.% W on the XRD patterns of the ZrC, Figure 3 depicts the effects of additions on the XRD patterns of the ZrC-20 vol.% W composite. We shown the appartion of two ceramic phases designed by tungsten carbide (W_2C and WC) composite, mainly increases the hardness of the composite because balistical composite need double hardeness and remaining no reacted W. In contrast, the peak positions of ZrC were higher than those of the starting ZrC powder, as addition of (20 vol.% W) are added, the peaks positions have no change (no shifting to the lower and higher side from the positions of the starting ZrC (Figure 3b).

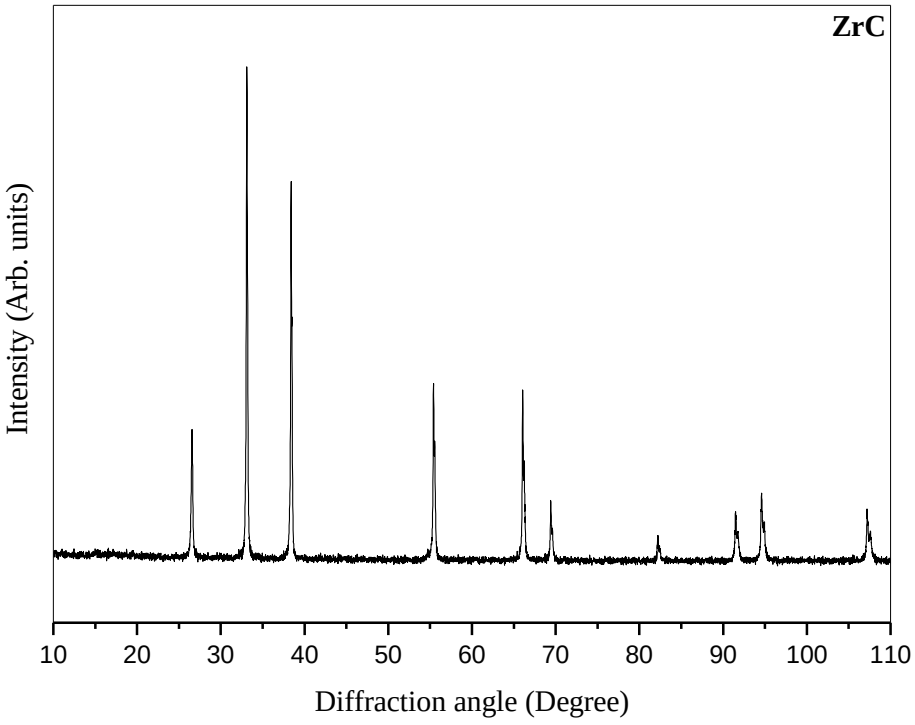
ZrC
Intensity (Arb. units)
10
20
30
40
50
60
70
80
90
100
110
Diffraction angle (Degree)

(a)

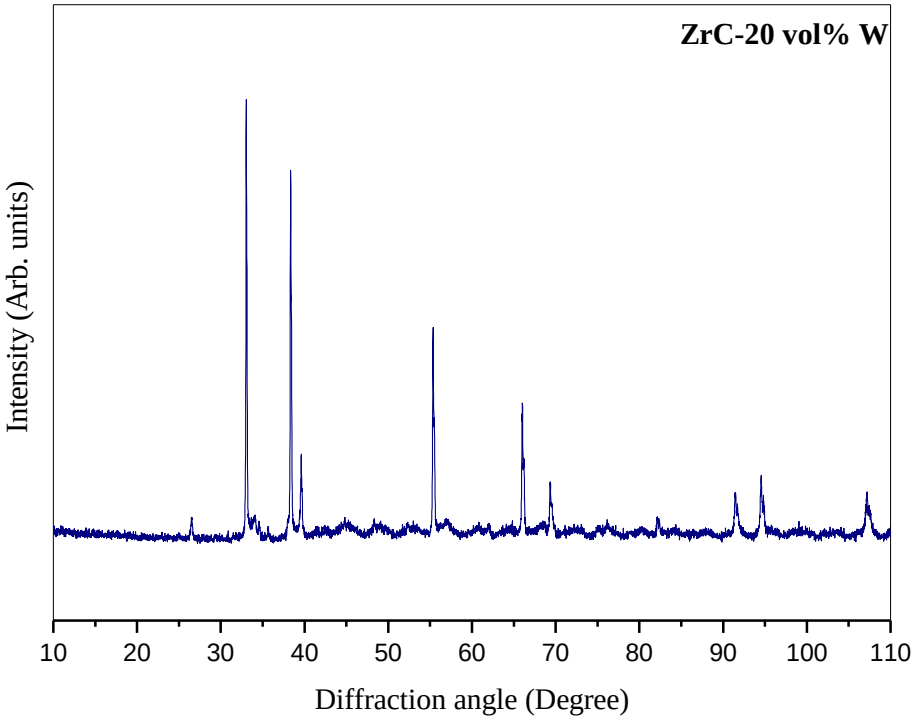
ZrC-20 vol% W
Intensity (Arb. units)
10
20
30
40
50
60
70
80
90
100
110
Diffraction angle (Degree)

(b)

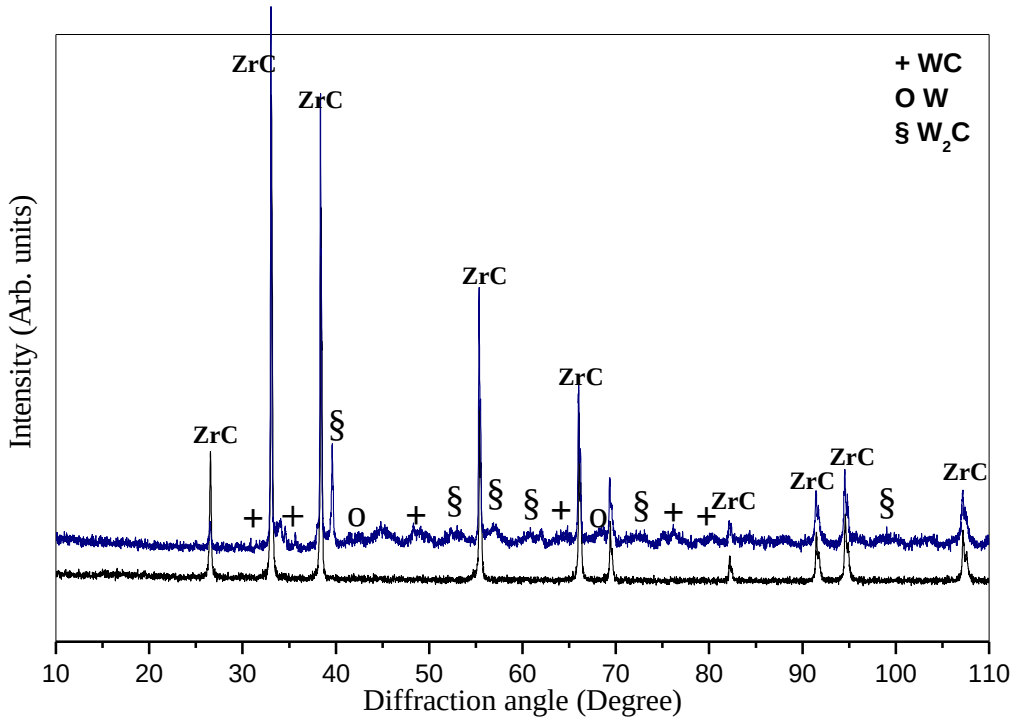

(c)

Figure 3 Spectra of ZrC carbide ceramic and composite ZrC-20Vol% W sintered by FAST-SPS-FCT technology at 1700 °C with die of 20 mm.

Figure 3a illustrated the ceramic zirconium carbide (ZrC) and the Figure 3b shown the effect of the addition of 20vol.% W into ZrC. The Figure 4a shows SEM imaging of the ZrC SPSed at 1700 °C, there are dark and bright regions that correspond of presence of (ZrC) SPSed at 1700 and 1800 °C, and WC dence withaout some pores areas, respectively. The relative densities reached 98.0 and 98.8 %, respectively. The addition of 20vol.% W clearly incressed the relative density by the formation of ternary phases composite.

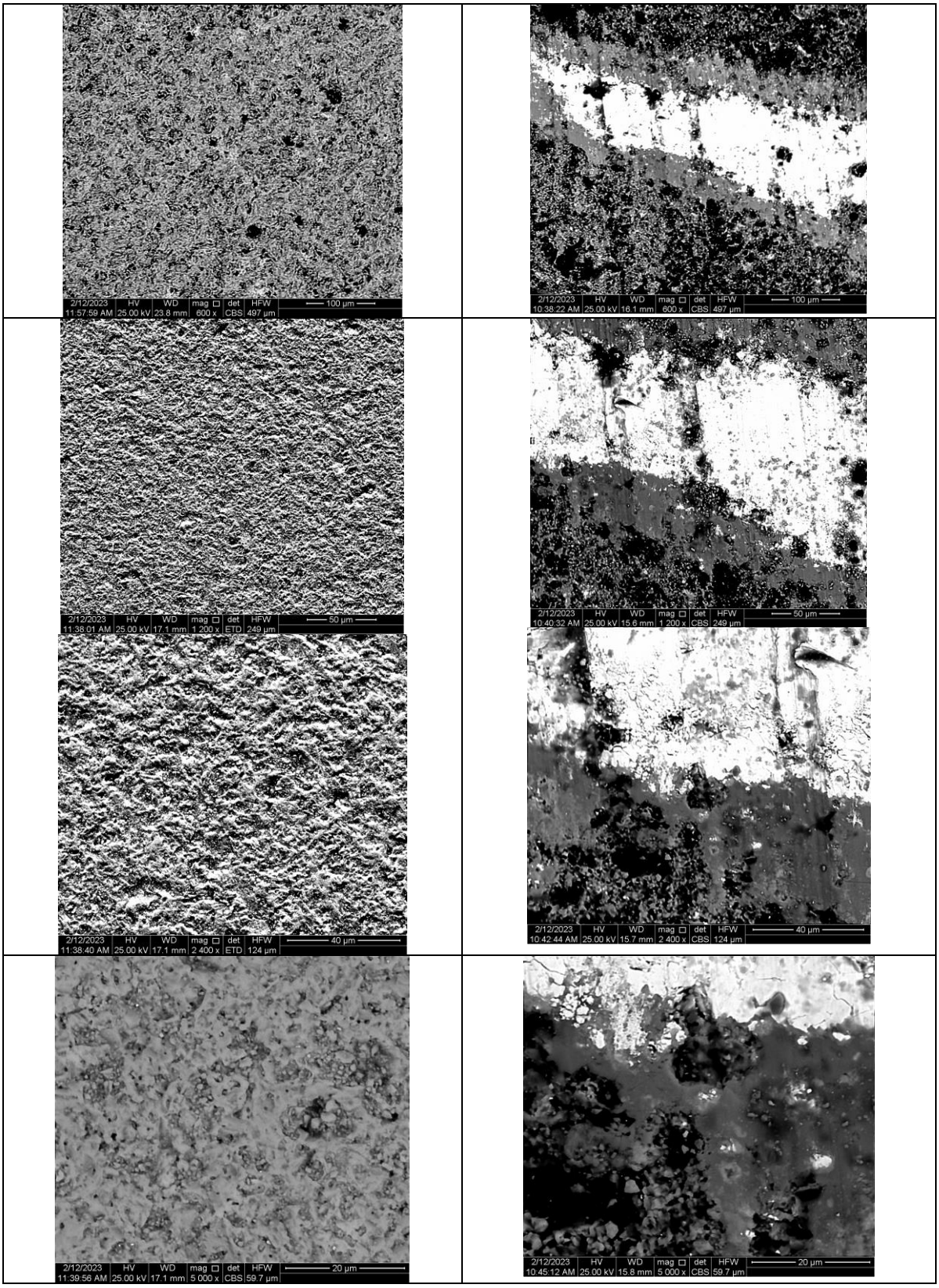
2/12/2023 11:57:59 AM HV 25.00 kV WD 23.8 mm mag 600 x det CBS HFW 497 µm 100 µm
2/12/2023 10:38:22 AM HV 25.00 kV WD 16.1 mm mag 600 x det CBS HFW 497 µm 100 µm
2/12/2023 11:38:01 AM HV 25.00 kV WD 17.1 mm mag 1 200 x det ETD HFW 249 µm 50 µm
2/12/2023 10:40:32 AM HV 25.00 kV WD 15.6 mm mag 1 200 x det CBS HFW 249 µm 50 µm
2/12/2023 11:38:40 AM HV 25.00 kV WD 17.1 mm mag 2 400 x det ETD HFW 124 µm 40 µm
2/12/2023 10:42:44 AM HV 25.00 kV WD 15.7 mm mag 2 400 x det CBS HFW 124 µm 40 µm
2/12/2023 11:39:56 AM HV 25.00 kV WD 17.1 mm mag 5 000 x det CBS HFW 59.7 µm 20 µm
2/12/2023 10:45:12 AM HV 25.00 kV WD 15.8 mm mag 5 000 x det CBS HFW 59.7 µm 20 µm

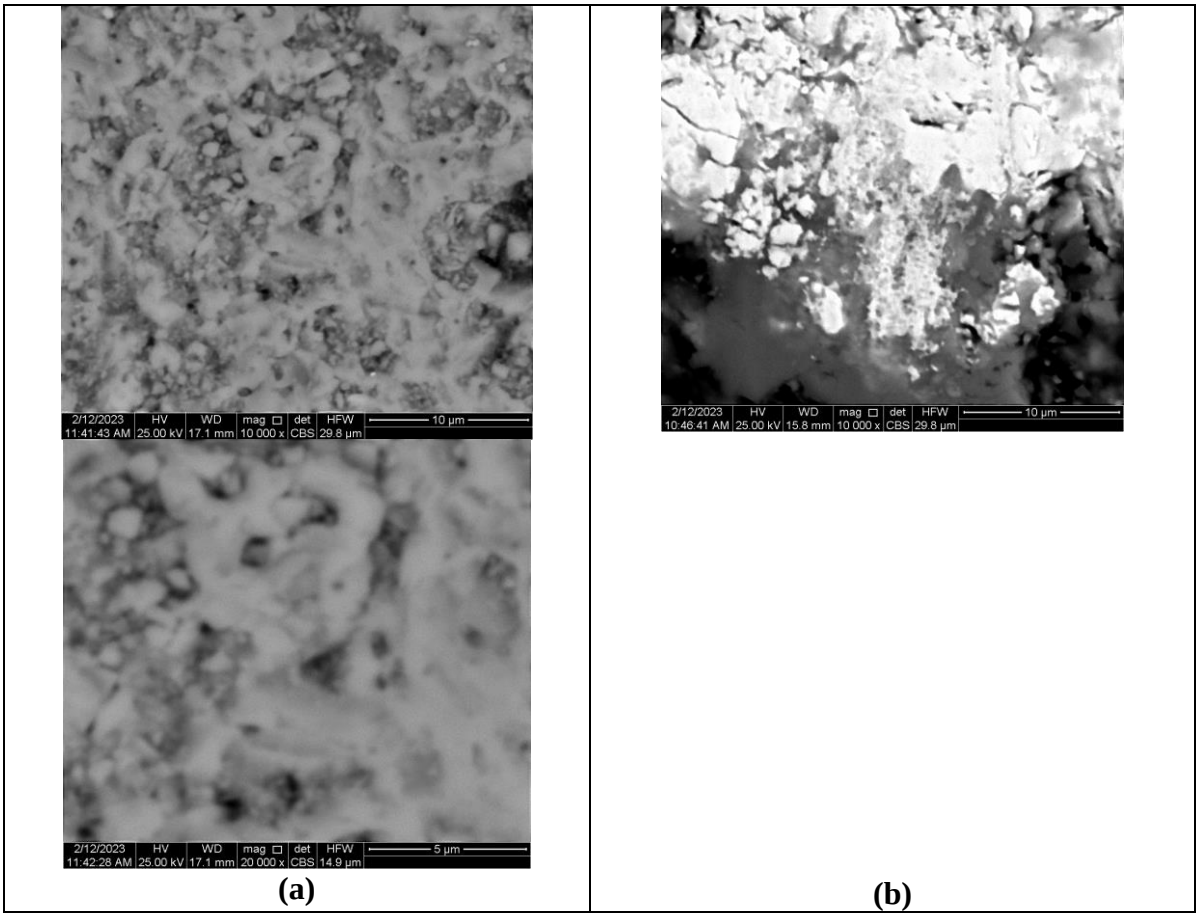

Figure 4 High magnification microstructural representative SEM of FAST-SPS-FCT sintered samples at 1700 °C. (a) Ceramic-carbide ZrC, (b) Composite ceramic-metal (ZrC-20 vol.% W).

To acquire the information on the distribution of various phases in the sintered samples, Energy-Dispersive X-ray Spectroscopy (EDS) analysis was performed on the samples. Although it is not possible to identify the phases by EDS directly, it is still very useful to detect elemental distribution of W, Zr, C in the samples. Thus, EDS analysis together with XRD results can provide more information regarding nature of FAST-SPS-FCT compacted and sintered powders. We presented in the Figure 5 compositions in differents important regions in the ceramic ZrC and the composite (MMC) ZrC-20vol.%W. The bring idea about the dynamic properties of the SPSed composite simulation of the ballistic performance by theoretical model based on the Heisenberg model will be estimated in the near coupled by the calculation of the thermo-mechanical properties in the SPS platform under ABAQUS.

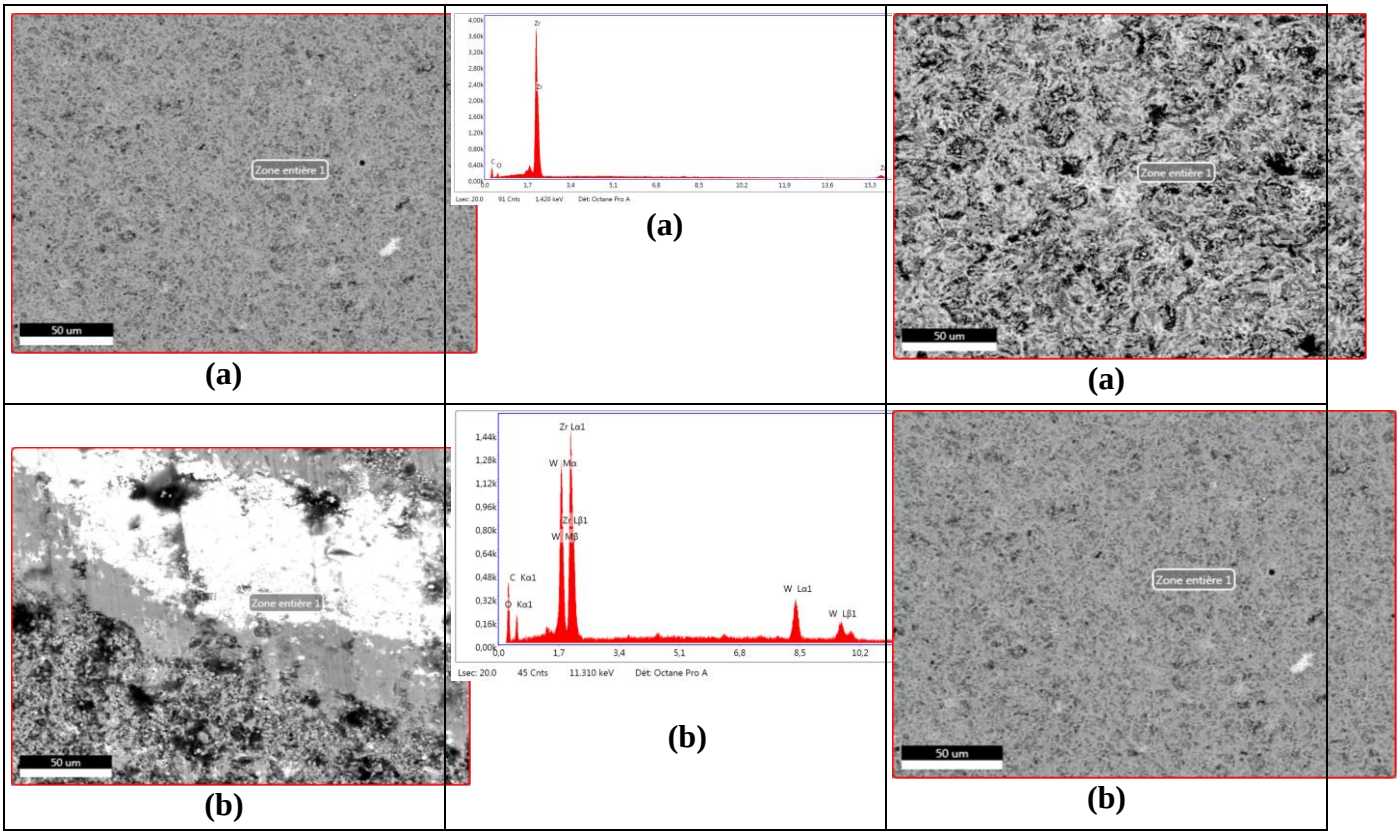

Figure 5 High magnification micro-structural representative FESEM image their corresponding elemental distribution (Zr, C, W) of FAST-SPS-FCT of polished and etched surface sintered at T=1700 °C. Its higher resolution global analysis EDS pics are presented.

3.1.3 Mechanical and physical properties

The physical and mechanical properties were listed in the Table 3.

Table 3 Physical parameters of ceramics and composites.

Parameters	**ZrC**	**ZrC-W**	**W**	**WC**
E (GPa)	440	522	410	650
γ	0.18	0.242	0.31	0.23
α ($x10^{-6}K^{-1}$)	6.74	7.32	3.62	1.3
HV (GPa)	25.5	26.10	3.03	34
$K_{IC\ (Mpa\ m^{1/2})}$	4.3	5.10	4.00	6.4
Theoretical density (g/cm^3)	6.73	9.78	15.25	15.7

The calculated paramaters like the R_{st} parameter represents the ability of a material to resist crack propagation, further damage and loss of strength with increasing severity of thermal shock. The greater R_{st} indicates better thermal shock resistance of a material. The thermal expention coefecient α from the literature are noted in the Table 4.

Table 4 Measured and calculated parameters of the ZrC Ceramic Carbide and ZrC-W Ceramic Metal Matrix.

	E (GPa)	α (10^{-6} K^{-1})	γ	R_{st} ($\mu m^{1/2}$ °C)	Relative density (%)
ZrC Carbide Ceramic	440	8.04	0.18	3194	98
ZrC-W Ceramic Metal Matrix composite	522	9.02	0.24		98.8
W	410	4.0	0.31		
WC	650		0.23		

4. CONCLUSIONS

In conclusion, this study focused on fabricating and characterizing tungsten-zirconium carbide (ZrC-W) cermet.

FAST-SPS-FCT technology is fast sintering process ; uniform sintering ; low grain growth (nano-grain materials may be prepared); compaction and sintering stages are combined in one operation; binders are not necessary; better purification and activation of the powder particles surfaces. The synthesis of ceramics, composites, FGMs and nano-composites is eaesly by FAST-SPS-FCT technology. It may be produced by self propagating high temperature synthesis (SHS) bat the product present bad relative density and should be folloyed by FAST-SPS-FCT for better density because the cenitic of sintering is improved. The FAST-SPS-FCT technology is the way to produce composites, nano-composite and nano-structuring of materials, also makes it possible to strengthen the material and armor materials to obtain a mechanical resistance exceeding all alloys in their conventional states to improuve ballistical protection. The addition of alloying elements and ceramic and the appropriate thermo-mechanical treatments are mastered and make it possible to obtain high mechanical resistance for the applications that require it. Nanostructuring and dispersion of the reinforcements will be carried out by high-energy grinding of the powder mixtures, and shaping by Spark Plasma Sintering, for the short cycles and low temperatures that the process allows. The precipitation at the origin of the structural hardening of this alloy will be the subject of particular interest. In this study it can summarize the following, according to the preliminary structural properties obtained results:

1- ZrC ceramic carbide was consolidated by FAST-SPS-FCT at 1700 °C using ZrC powders has achieved relative densities over 98%.

W–ZrC composite having ZrC composition 80 vol.% were densified and SPSed to relative densities over 98.8%.

2-At sintering temperatures 1700 °C, the sintered samples were mixed phases of Zr-rich (Zr)C formed with a uniform morphology.

3-The apparition of the secondaire WC and ternary W_2C phases in the composite incresse certainly the hardness of the composite (double hardeness for balistical materials).

3- It is now confirmed that the additions of tungsten (W) have maked change on the lattice parameters of ZrC-20 vol.% W in solid solution and incresse the density of the composite and mainly the mechanical properties.

The theoretical simulation and experimental ballistic performance by dynamic testing apparatus of the manufactured composite ceramic-metal, HV and K_{IC} measurement in addition thermo-mechanical modeling in situ FAST-SPS-FCT plate form will be performed in the near future. The resulting composites exhibited distinct properties for ballistical composite, FGMS and cermet armor.

Acknowledgments

The present work was supported by the Algerian Ministerium of Higher Education and Scientific Research (MESRS, Algiers) and the PRFU project entitled: Synthesis by FAST-SPS-FCT, Characterization and Thermo-Mechanical Modeling of Cermet, Nano-composite and FGMs For Ballistic Protection, under contract N°A11N01UN240120220005 at the University of 08 May 1945, Guelma. These supports are gratefully appreciated. Finally, I am grateful to Eberhard Burkel (Rostock, Germany, 2013), Pr. Giacomo Gao (Cagliari, Italy, 2014), Pr. Jacques Guillome Noudem, Pr. David Houivet (Cean and Cherbourg-Octeville, France, 2016) and Pr. Frederick Bernard (Dijon, France, 2018) for having made available to me the FAST-SPS-FCT technology sintering apparatus and the consumable graphit and raw materials.

References

[1] R. Zhang, B. Han, L. Li, ZN. Zhao, Q. Zhang, QC. Zhang, Compos Struct 227 (2019) 111258
[2] J. Marx, M. Portanova, A. Rabiei, Compos. Struct 225 (2019) 111032
[3] W. Liu, Z. Chen, Z. Chen, X. Cheng, et al., Mater Des 87 (2015) 421
[4] PJ. Hazell, Armour: materials, theory, and design. Boca Raton, FL, USA: CRC Press; 2015
[5] WA. Gooch, BHC. Chen, MS. Burkins, R. Palicka, JJ. Rubin, Mater Sci Forum 1999
[6] S. Li, G. Wang, K. Zhang, et al., J Alloys Compd 950 (2023) 169948
[7] X. Zhang, Q. Meng, K. Zhang, et al, Chem Eng J 463 (2023) 142378
[8] ESC. Chin, Mater Sci Eng, A 259 (1999) 15561
[9] HA. Bruck, Int J Solid Struct 37 (2000) 638395
[10] A. Pettersson, P. Magnusson, P. Lundberg, M. Nygren, Int J Impact Eng 32 (2005) 38799
[11] JW. McCauley, GD. Andrea, K. Cho, MS. Burkins, Report Documentation of US Army Research Laboratory; 2006
[12] N. Gupta, B. Basu, V. Prasad, M. Vemuri, Defence Sci J 62 (2012) 3829
[13] E. Balci, B. Sarikan, M. Ubeyli, Kovove Mater 51 (2013) 25762
[14] M. U¨ beyli, E. Balci, B. Sarikan, Mater Des 56 (2014) 316
[15] ZL. Chao, LT. Jiang, GQ. Chen, J. Qiao, Compos B Eng 161 (2019) 62738
[16] B. Koohbor, A. Kidane, Mater Des 102 (2016) 15161
[17] K. Arslan, R. Gunes, Compos Struct 202 (2018) 30412
[18] M. Aydin, MK. Apalak, Mater Sci Eng, A 671 (2016) 10717
[19] M. Aydin, MK. Apalak, J Compos Mater 54 (2020) 3967
[20] S. Chi, YL. Chung, Eng Fract Mech 70 (2003) 122743
[21] A. Berezovski, J. Engelbrecht, Maugin GA, Eur J Mech Solid 22 (2003) 25765
[22] DW. Templeton, TJ. Gorsich, TJ. Holmquist, Report U.S.A; 2006
[23] J. Jovicic, A. Zavaliangos, F. KO, Modeling, Compos. A Appl. S. 31 (2000) 77384
[24] Y. Li, KT. Ramesh, ESC. Chin, Int J Solid Struct 38 (2001) 604561
[25] DS. Kleponis, Al. Mihalcin, GL. Filbey, U.S. Army Research Laboratory; 2005
[26] Y. Wang, Q. Liu, Y. Li, Q. Shen, J. Phys. Confe. Seri. 419 (2013) 012026
[27] WR. Wang, HF. Xie, L. Xie, HL. Li, X. Yang, YN. Shen, I. J. Min. Met. Mater. 25 (2018) 13208
[28] R. Gunes, M. Aydin, Compos Struct 92 (2010) 244556
[29] R. Gunes, M. Aydin, MK. Apalak, JN. Reddy, Compos Struct 93 (2011) 8609
[30] R. Gunes, M. Aydin, MK. Apalak, et al. Compos B Eng 59 (2014) 2132
[31] T. Zhang *et al.*, Mater. Sci. Eng. A 527 (2010) 4914
[32] M. Roosta *et al.*Int. J. Refract. Met. Hard Mater. 37 (2013) 29
[33] J.H. Kim *et al.*, J. Alloys Compd. 653 (2015) 528
[34] M. Roosta *et al.*, Int. J. Refract. Met. Hard Mater. 29 (2011) 710
[35] A. Moradkhani *et al.*, Eng. Fract. Mech. 191 (2018) 446

[36] R.K. Mudanyi *et al.* Int. J. Refract. Met. Hard Mater. 94 (2021) 105411
[37] W.G. Fahrenholtz *et al.*, Scr. Mater. 94 (2017) 129
[38] H. Wang *et al.*, Int. J. Refract. Met. Hard Mater. 55 (2010) 572
[39] C.W. Bale *et al.*, Calphad. 33 (2002) 295
[40] M. Roosta *et al.* Int. J. Refract. Met. Hard Mater. (2011) 8327
[41] B. Bendjemil et al., Exp. Theo. NANOTECHNOLOGY 1 (2017) 49
[42] D. Zhanga, Ch. Kenel, M. Caccia, K. H. Sandhage, D. C. Dunanda, J. Alloys Comp. 1 (2021) 100018
[43] Toufik Nouri, Friha Khelfaoui, Kadda Amara, Abdelmadjid Bouhemadou, Fadila Belkharroubi, Y. Al-Douri, Physica B 678 (2024) 415780
[44] Djamel Allali, Bouhemadou Abdelmadjid, Saad Essaoud Saber, Deghfel Bahri, Fares Zeraga, Rabie Amari, Missoum Radjai, Saad Bin-Omran, Khenata Rabah, Y. Al-Douri, Computational Condensed Matter 38 (2024) e00876
[45] Y. Al-Douri, Mohammad Mansoob Khan, James Robert Jennings, Journal of Materials Science: Materials in Electronics 34 (2023) 993
[46] X. Zhang, N. Liu, Int. J. Refract. Met. Hard Mater. 26 (2008) 575
[47] Abraham George, Exp. Theo. NANOTECHNOLOGY 8 (2024) 1
[48] J. G. Kim, P. Tan, Exp. Theo. NANOTECHNOLOGY 8 (2024) 17
[49] Maria S. da Dunla, Exp. Theo. NANOTECHNOLOGY 8 (2024) 23